

# Technical note: Geodynamic Thermochronology (GDTchron) – A Python package to calculate low-temperature thermochronometric ages from geodynamic numerical models

Dylan A. Vasey<sup>1</sup>, Peter M. Scully<sup>1</sup>, John B. Naliboff<sup>2</sup>, Sascha Brune<sup>3,4</sup>

5 <sup>1</sup>Department of Earth and Climate Sciences, Tufts University, Medford, MA, 02155, USA

<sup>2</sup>Department of Earth and Environmental Science, New Mexico Institute of Mining and Technology, Socorro, NM, 87801, USA

<sup>3</sup>GFZ Helmholtz Centre for Geosciences, Telegrafenberg, 14473 Potsdam, Germany

<sup>4</sup>Institute of Geosciences, University of Potsdam, 14476 Potsdam-Golm, Germany

10 *Correspondence to:* Dylan A. Vasey (dylan.vasey@tufts.edu)

## Abstract.

Low-temperature thermochronology provides a powerful means of extracting quantitative information on the thermal evolution of different tectonic settings from rocks exposed at the surface of the Earth. Geodynamic numerical models enable tracking the entire thermal structure of simulated tectonic settings throughout their evolution. Despite the highly complementary nature of these two approaches, few geodynamic modeling studies have used the thermal information in models to predict thermochronometric ages as a means of comparing model results with observational data. Here, we present Geodynamic Thermochronology (GDTchron): an open-source Python package designed to forward model large numbers of low-temperature thermochronometric ages from time-temperature paths output by geodynamic numerical models. This package uses existing techniques to estimate apatite (U-Th)/He, apatite fission track, and zircon (U-Th)/He ages from time-temperature paths in a parallelized workflow that enables faster computation on multicore processors and high-performance computing systems. The workflow is built on typical output files from geodynamic models containing particle location, time, and temperature, and we use an interpolation scheme to allow new particles to inherit the thermal histories of their nearest neighbors. GDTchron can be applied to any tectonic setting, though for results to be comparable to nature, geodynamic models should carefully account for erosion and sedimentation. We demonstrate the functionality of this software with a highly simplified geodynamic model of exhumation and a more complicated model of rift-inversion orogenesis with the aim of encouraging community participation in broadening future development.

15  
20  
25

## 1 Introduction

Interpretation of low-temperature thermochronometric data and ages has become increasingly sophisticated in recent years, enabling extraction of more detailed information on the thermal history of many tectonic settings from the (U-Th)/He and fission track systems (e.g., [van der Beek and Schildgen, 2023](#); [Enkelmann and Garver, 2016](#); [Flowers and Peak, 2025](#); [Fosdick](#)

30

~~et al., 2024; Gallagher and Parra, 2020; Guenther, 2021; Ketcham, 2024)(e.g., van der Beek and Schildgen, 2023; Enkelmann and Garver, 2016; Flowers and Peak, 2025; Fosdick et al., 2024; Gallagher and Parra, 2020; Guenther, 2021; Ketcham, 2024).~~

35 Simultaneously, advances in geodynamic numerical modeling have enabled high-resolution simulations of these tectonic settings with increasingly realistic approximations of a range of geologic processes (e.g., Balázs et al., 2021; Fraters and Billen, 2021; Glerum et al., 2024; Jourdon and May, 2022; Neuharth et al., 2022; Wolf et al., 2021; Zwaan et al., 2025). However, the non-uniqueness of the tectonic processes and thermal histories that produce thermochronometric data and the difficulties of validating geodynamic models with observational data remain major challenges. Stronger interaction between these fields has the potential to improve the interpretive capabilities of each. Geodynamic models track temperature over time with complete knowledge of the processes that impact the temperatures recorded, while thermochronometric data at the surface of  
40 the Earth are quantitative constraints against which geodynamic models could be validated.

~~Although thermokinematic models have often been used to predict low-temperature thermochronometric ages (e.g., Almendral et al., 2015; Braun, 2003; Braun et al., 2012; Capaldi et al., 2022; Curry et al., 2021; Erdős et al., 2014; Gilmore et al., 2018), only a few studies have used the outputs of fully geodynamic models to predict such ages for comparison with natural systems~~

45 ~~Although thermokinematic models have often been used to predict low-temperature thermochronometric ages (e.g., Almendral et al., 2015; Braun, 2003; Braun et al., 2012; Capaldi et al., 2022; Curry et al., 2021; Erdős et al., 2014; Gilmore et al., 2018; Lock and Willett, 2008), only a few studies have used the outputs of fully geodynamic models to predict such ages for comparison with natural systems (Jourdon et al., 2018; Ternois et al., 2021). The fundamental difference between these two types of models lies in how material movement (e.g., rock uplift) is handled. In thermokinematic models, material movement, generally restricted to the uppermost crust, is fully prescribed as a model input, and the model uses this motion in combination with a temperature model and often a landscape evolution model to test the impact of a given exhumation history on thermochronometric ages (e.g., Braun, 2003; Braun et al., 2012; Ehlers, 2023). By contrast, in geodynamic models, material movement is instead a response to dynamic forcings, which may include far-field tectonic stresses simulated as velocities imposed on the model boundaries, and/or forcings internal to the model such as mantle convection and slab pull (e.g., Burkett and Billen, 2009; Coltice et al., 2019; Duretz et al., 2011). To realistically approximate the effects of such forcings, geodynamic models generally have larger model domains (100s to 1000s of km in each dimension) and include complex rheological parameters simulating the response of multiple materials to stress under varying conditions. Thus, while thermokinematic models do an excellent job of testing the effects of near-surface rock uplift, isotherm advection, and topographic evolution on thermochronometric ages, only geodynamic models can test the effects of variable tectonic regimes and evolving material properties on exhumation itself.~~

60

~~Here, we present Geodynamic Thermochronology (GDTehron): a Python package designed to facilitate the forward modeling of large numbers of low-temperature thermochronometric ages using time-temperature (t-T) histories extracted from geodynamic numerical models (Vasey and Scully, 2025). The fundamental difference between these two types of models lies~~

Field Code Changed

65 in how material movement (e.g., rock uplift) is handled. In thermokinematic models, material movement, generally restricted  
to the uppermost crust, is fully prescribed as a model input, and the model uses this motion in combination with a temperature  
model and often a landscape evolution model to test the impact of a given exhumation history on thermochronometric ages  
(e.g., Braun, 2003; Braun et al., 2012; Ehlers, 2023). By contrast, in geodynamic models, material movement is instead a  
70 response to dynamic forcings, which may include far-field tectonic stresses simulated as velocities imposed on the model  
boundaries and/or forcings internal to the model such mantle convection and slab pull (e.g., Burkett and Billen, 2009; Coltice  
et al., 2019; Duretz et al., 2011). To realistically approximate the effects of such forcings, geodynamic models generally have  
larger model domains (100s to 1000s of km in each dimension) and include complex rheological parameters simulating the  
response of multiple materials to stress under varying conditions. Thus, while thermokinematic models do an excellent job of  
75 testing the effects of near-surface rock uplift, isotherm advection, and topographic evolution on thermochronometric ages, only  
geodynamic models can test the effects of variable tectonic regimes and evolving material properties on exhumation itself.

Here, we present Geodynamic Thermochronology (GDTchron): a Python package designed to facilitate the forward modeling  
of large numbers of low-temperature thermochronometric ages using time-temperature (t-T) histories extracted from  
geodynamic numerical models (Vasey et al., 2026). Our package employs existing diffusion and annealing models  
80 implemented in the widely-used HeFTy inverse modeling program (Ketcham et al., 1999, 2000, 2011; Ketcham,  
2005)(Ketcham et al., 1999, 2000, 2011; Ketcham, 2005) to estimate apatite (U-Th)/He (AHe), apatite fission track (AFT),  
and zircon (U-Th)/He (ZHe) ages from prescribed t-T paths in a parallelized workflow that can take advantage of  
multiprocessing and high-performance computing (HPC). The package contains tools for extracting t-T paths for unique  
85 particles from commonly used geodynamic model output file formats across multiple timesteps, and an interpolation scheme  
allows particles created during a model run to inherit thermal information from their nearest neighbors. We present two  
example geodynamic models illustrating the use for this package: 1) a highly simplified model of exhumation that illustrates  
the expected behavior of the AHe, AFT, and ZHe systems and 2) a more complex model of rift-inversion orogenesis where  
geodynamic processes are coupled with hillslope diffusion, the stream power law, and marine transport/deposition. The results  
contain thermal information about both rift-related and orogenic exhumation. We note that GDTchron is currently an early  
90 version of software that we envision as a community-developed tool, and we outline current limitations and paths forward for  
future development.

## **2 Forward modeling of (U-Th)/He and apatite fission track ages**

At the core of GDTchron are modules designed to forward model low-temperature thermochronometric ages for individual  
mineral grains given a time-temperature history. These modules follow the approaches described in Ketcham (2005), and the  
95 examples from that study are included as benchmark tests in the GDTchron Python package. The employed kinetic models  
(Farley, 2000; Ketcham et al., 1999; Reiners et al., 2004) are relatively simple, and there have been notable updates and

improvements over the past twenty years that address the effects of crystal composition and complex, multi-part thermal histories on age (e.g., Enkelmann and Garver, 2016; Flowers et al., 2009, 2023a, b; Guentner, 2021; Guentner et al., 2013, 2014; Ketcham, 2019; Ketcham et al., 2007; Shuster et al., 2006; Tamer and Ketcham, 2020). Nevertheless, these forward models provide first-order ages that capture the impact of thermally controlled He diffusion and fission track annealing. They are also sufficiently computationally efficient to evaluate the large number of thermal histories output by geodynamic models and are often appropriate for the relatively simple thermal histories captured within such models. (e.g., Enkelmann and Garver, 2016; Flowers et al., 2009, 2023a, b; Guentner, 2021; Guentner et al., 2013, 2014; Ketcham, 2019; Ketcham et al., 2007; Shuster et al., 2006; Tamer and Ketcham, 2020). Nevertheless, these forward models provide computationally efficient first-order ages and track length distributions that capture the impact of thermally controlled He diffusion and fission track annealing. For relatively short-lived thermal histories involving rapid cooling events, such ages and distributions do not deviate significantly from those predicted by more updated kinetic models, and many geodynamic models are designed to produce such relatively simple thermal histories.

The forward models of GDTchron are open-source and contained within a publicly hosted Python package. They can thus be easily extended by the community to allow for more complex kinetics in the future, and they can also be employed for education on the fundamentals of low-temperature thermochronology. Note that, because uncertainties reported for observed low-temperature thermochronometric ages are typically analytical uncertainties, our model ages based on predefined thermal histories are reported without uncertainties.

### 2.1 Apatite and zircon (U-Th)/He

We model the (U-Th)/He system by combining ingrowth of He into a mineral crystal via decay of  $^{238}\text{U}$ ,  $^{235}\text{U}$ , and  $^{232}\text{Th}$  with temperature-controlled diffusion of He out of the crystal lattice. We use the finite difference solution to the diffusion equation outlined by Ketcham (2005) to approximate He diffusion in a sphere. This approach divides the radius of the sphere into a series of nodes, with loss of He at each node a function of temperature and distance from the edge of the sphere. The concentration of He at each node is then scaled to the relative volume of a spherical shell corresponding to the position of the node along the radius. The He concentrations in each shell are summed to obtain the total He within the sphere, which is then used to calculate a (U-Th)/He age. The effect of  $\alpha$  ejection on He concentration and the resulting age is approximated by reducing the amounts of U and Th used to model He ingrowth by a factor determined by the distance from the edge of the sphere and the  $\alpha$  stopping distance for the mineral, after Ketcham et al. (2011). The diffusivity of He within a particular mineral system is modeled using empirically-derived frequency factors ( $D_0$ ) and activation energies ( $E_a$ ) reported for apatite (Farley, 2000) and zircon (Reiners et al., 2004).

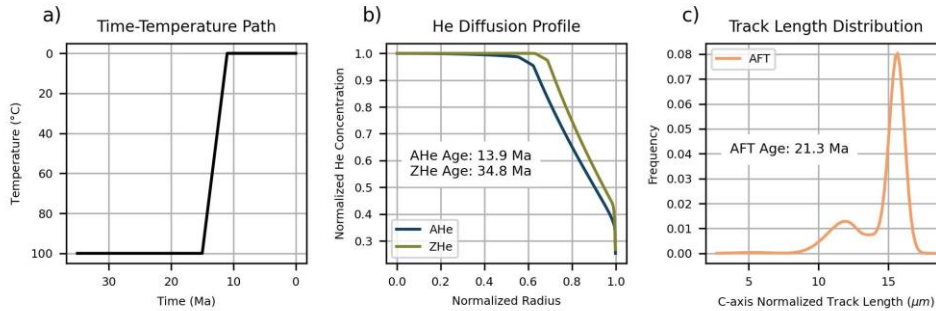
## 2.2 Apatite fission track

The apatite fission track (AFT) system is modeled by simulating annealing of fission tracks within an apatite crystal at a given temperature for each timestep within a time-temperature path, following the approach outlined in Ketcham (2005). Annealing is approximated using the fanning curvilinear model of Ketcham et al. (1999), which relates normalized c-axis projected fission track lengths to time and temperature via a set of six fitted parameters and results in in slightly curved lines of constant annealing that fan out from a single point on an Arrhenius plot. For each timestep, new normalized c-axis projected lengths are calculated based on the average temperature of the timestep, the length of the timestep, and the equivalent time needed to produce the initial normalized c-axis projected lengths prior to the timestep at the temperature of the timestep. The c-axis projected lengths are adjusted based on an input etch pit diameter ( $D_{\text{pit}}$ ) that, which approximates chemical variations within apatite crystals, and converted to normalized fission track densities (Ketcham et al., 2000, 1999; Ketcham, 2005). The densities are summed to calculate a total AFT age, and the normalized c-axis projected lengths are converted to mean c-axis projected lengths and combined in order to visualize the shape of the length distributions.

Field Code Changed

## 2.3 Example forward models from a time-temperature path

Figure 1 shows a prescribed time-temperature path for a sample that resides at 100°C from 35 Ma (megaannums – millions of years ago) to 15 Ma, cools at a rate of 25°C/Myr (megayears – million years) from 15 Ma to 11 Ma, and then remains at 0°C from 11 Ma to 0 Ma. This path was chosen to illustrate the expected effects of rapid, monotonic cooling from a temperature that is above the partial retention zone for the apatite (U/Th)/He (AHe) system (~30-90°C), within the partial annealing zone of the apatite fission track (AFT) system (~60-110°C), and below the partial retention zone of the zircon (U-Th)/He (ZHe) system (~100-220°C). For the AHe system warmer than the partial retention zone for the apatite (U/Th)/He (AHe) system (~55-80°C), within the partial annealing zone of the apatite fission track (AFT) system (~60-110°C), and cooler than the partial retention zone of the zircon (U-Th)/He (ZHe) system (~160-200°C) (Reiners et al., 2005). For the AHe system, this results in an age of 13.9 Ma, which represents the rapid cooling of the sample through the entire AHe partial retention zone between 15 Ma and 11 Ma. By contrast, for the zircon (U-Th)/He (ZHe) system, this path results in an age of 34.8 Ma, corresponding to nearly the full duration of the 35 Myr history, given that the sample remains at a temperature below cooler than the ZHe partial retention zone throughout this history. The apatite fission track (AFT) age is 21.3 Ma, an intermediate value between the 35 Ma start of the path and the 15 Ma to 11 Ma cooling period, indicating that the sample stayed within the AFT partial annealing zone until 15 Ma and then cooled below the partial annealing zone. This example indicates how ages within these systems will produce distinctly different ages from the same time-temperature history due to their variable kinetics.



155

**Figure 1:** Example forward modeling results for a single time-temperature path. **a)** Time-temperature path over 35 Myr with cooling from 100°C to 0°C from 15 Ma to 11 Ma. **b)** He diffusion profiles and ages after 35 Myr for apatite (AHe) and zircon (ZHe) grains with 100 ppm each of U and Th and a radius of 50  $\mu\text{m}$ . **c)** C-axis normalized track length distributions and age for apatite (AFT) grain with  $D_{\text{par}}$  of 1.75 after 35 Myr.

### 160 3 Scaling for large numbers of time-temperature paths

The primary new functionality in GDTchron is the ability to efficiently use the large number (thousands to millions) of time-temperature (t-T) paths output by geodynamic models to predict synthetic AHe, AFT, and ZHe ages throughout the model domain and at each timestep of the model run.

#### 3.1 Parallelized forward modeling

165 To make use of multi-core processors available on high-performance computing (HPC) nodes and personal computers, we parallelize our forward models using the Python package Joblib. This allows the processor to calculate multiple t-T paths simultaneously, depending on the number of cores available, in order to speed up the calculation of many t-T paths. Within this parallelized framework, the choice of batch size can be particularly important for maximizing model efficiency. Batch size refers to the number of jobs (e.g., t-T paths) sent to each worker (i.e., core) at once; higher batch size decreases the number of  
 170 times jobs need to be routed to the worker while increasing the amount of computation routed each time. We find that optimal batch size varies significantly depending on the length of the t-T path, the number of total paths, and the device used. For geodynamic model outputs, where the number of paths is usually greater than 10,000 and the individual calculations at each timestep are relatively cheap, batch sizes of ~100 to 1,000 generally lead to the most efficient parallelization.

175 In an ideally parallelized workflow, doubling the number of cores will halve the computation time, though the overhead required to set up parallelization, as well as the increased memory usage of parallelized workflows, will dampen this effect. Figure 2 shows scaling results up to 64 cores on a node on the Tufts [University](#) HPC cluster for prediction of 96,000 AHe ages

for t-T paths with random temperatures between 0°C and 75°C assigned every 100,000 years over 40 Myr. Scaling results are generally good, with the computation taking 1,534 seconds on 1 core and 37 seconds on 64 cores (Figure 2). The resulting ages are generally between 10 Ma and 22 Ma, reflecting t-T paths partially in and partially **below cooler than** the AHe partial retention zone (e.g., [Reiners et al., 2005](#); Reiners and Brandon, 2006).

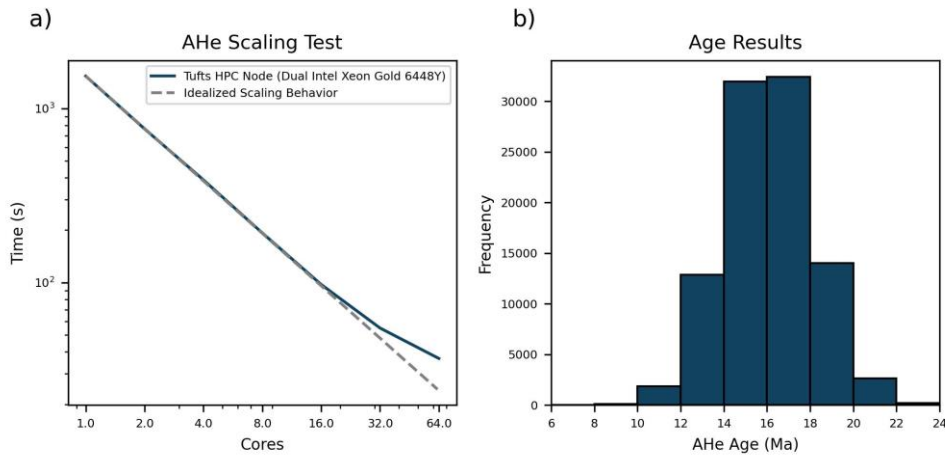


Figure 2: a) Scaling results for Tufts

[University HPC node producing apatite \(U-Th\)/He \(AHe\) ages from 96,000 synthetic time-temperature \(t-T\) paths with pseudorandom temperatures between 0°C and 75°C assigned every 100,000 years over 40 Myr. b\) Histogram of resulting AHe ages produced from the 96,000 t-T paths.](#)

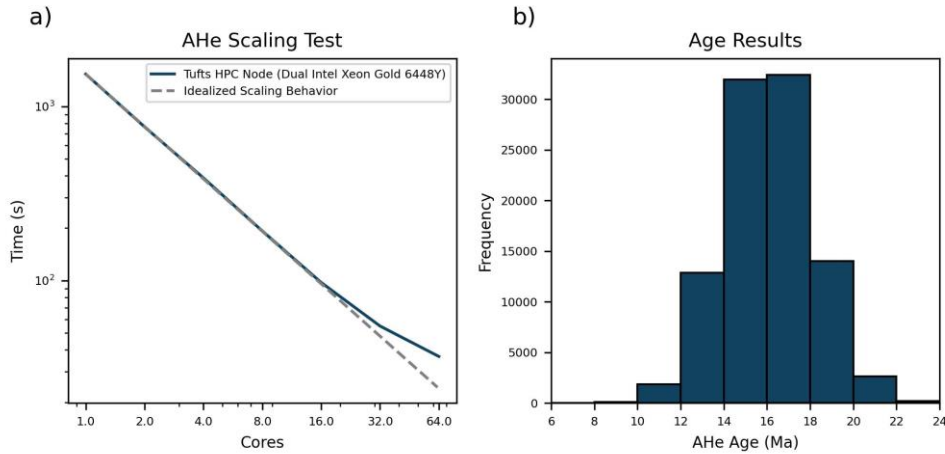
The computing resources needed to use GDTchron will depend on the scale of the input geodynamic model and the number of particles for which the user needs predicted ages. A complex 2D geodynamic model like the rift-inversion model presented in Section 4 may contain a few million particles, which would likely require tens of hours on **an** HPC node like the one used for our scaling test to produce AHe, AFT, and ZHe ages for all particles at all timesteps. The resources needed can be reduced by only running particles from a portion of the model domain (e.g., only particles that come near the surface where **any** daughter product can be accumulated) or a portion of the runtime that is of interest. Future development efforts will aim to further increase the efficiency of GDTchron and **increase** the degree to which high-resolution results can be obtained using a personal computer.

Formatted: English (United Kingdom)

Formatted: English (United Kingdom)

Field Code Changed

Formatted: Font: Bold



195 **Figure 2:** a) Scaling results for Tufts HPC node producing apatite (U-Th)/He (AHe) ages from 96,000 synthetic time-temperature (t-T) paths with pseudorandom temperatures between 0°C and 75°C assigned every 100,000 years over 40 Myr. b) Histogram of resulting AHe ages produced from the 96,000 t-T paths.

Formatted: Font: Bold

### 3.2 Processing outputs from geodynamic modeling software

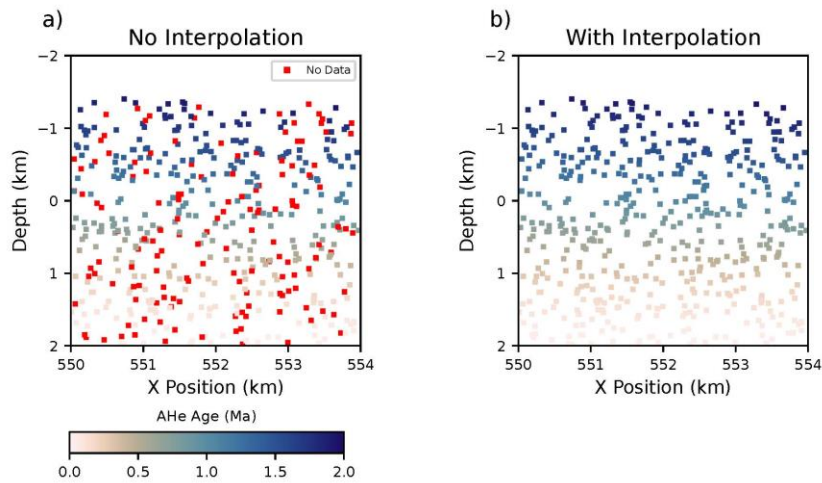
200 Typical outputs embedded within geodynamic models may include temperature, pressure, velocity, strain, strain rate, viscosity, density, heat flux, cohesion, and angle of internal friction, in addition to other fields that are of interest to the specific application of the model. These values are typically output at evenly spaced timesteps and are frequently embedded within complex data structures that can accommodate the irregular geometries and many parameters tracked in such models. GDTchron is currently designed to work with file formats from the Visualization Toolkit (VTK) software, which is commonly  
 205 used for visualization of three-dimensional scientific data. These file formats are the standard output of the open-source geodynamic modeling software ASPECT (Advanced Solver for Problems in Earth's Convection and Tectonics; Bangerth et al., 2024; Heister et al., 2017; Kronbichler et al., 2012), as well as other geodynamic codes (e.g., LaMEM; Kaus et al., 2016; pTatin3D; May et al., 2014; ELEFANT; Thieulot, 2014)(e.g., LaMEM; Kaus et al., 2016; pTatin3D; May et al., 2014; ELEFANT; Thieulot, 2014). For use with ASPECT, GDTchron requires that models track material properties using particle-  
 210 in-cell methods (e.g., Gassmöller et al., 2018, 2019), since this allows the temperature of the same particle to be tracked across multiple timesteps.

GDTchron uses the Python-based visualization package PyVista (Sullivan and Kaszynski, 2019) to extract all particle identification numbers and their corresponding temperatures from the output VTK file of each ASPECT timestep. The

215 temperatures and time elapsed between timesteps are distributed to the forward models described in Section 2 to update the  
He profile or fission track length distribution for that particle and to calculate a thermochronometric age at that timestep. The  
ages are added as a new scalar field to the imported VTK file. The He profile or length distribution for each particle is retained  
and then used as the starting point for the same particle at the subsequent timestep, preventing duplicate computation and  
allowing ages to be calculated at all timesteps for all particles that are present throughout the model run.

220

In particle-in-cell geodynamic models, individual particles are added and deleted as necessary to achieve optimal particle  
density in each cell during the model run. This results in the frequent addition of particles with no prior thermal history. We  
address this problem at a first-order level with an interpolation scheme using  $k$ -d trees (Bentley, 1975; Virtanen et al.,  
2020)(Bentley, 1975; Virtanen et al., 2020), in which new particles are assigned the He profile or track length distribution of  
225 the particle with the needed information that they are closest to in terms of physical difference (Figure 3). We note that using  
such interpolation both increases computation time and introduces the possibility of assigning a particle a thermal history that  
it would not have experienced, particularly in the case of particles that are added near the surface of a geodynamic model to  
approximate sedimentation, as discussed in Section 5. As a result, this is an optional component of the software that can be  
turned off such that only particles present at all timesteps are assigned thermochronometric ages.



230

**Figure 3:** Individual particles with assigned apatite (U-Th)/He (AHe) ages after 36 Myr of a rift inversion model. **a)** With no interpolation of thermal history, particles added during the model run have no result (red). **b)** With interpolation as described in the text, all particles are assigned a thermal history and AHe age. Colormaps here and below from Cramer et al. (2020)(2020).

### 3.3 Application to a simple exhumation model

To illustrate the above functionality, we designed a simple particle-in-cell ASPECT model consisting of a two-dimensional box 100 km wide and 20 km deep (Figure 4). The material in this box is given a density of  $2.8 \text{ g/cm}^3$  and a thermal conductivity of  $2.5 \text{ W/m} \cdot \text{K}$  to approximate the upper crust. The model is assigned a conductive geothermal gradient (Chapman, 1986) corresponding to a basal heat flow of  $85 \text{ mW/m}^2$  and radiogenic heat production of  $1 \times 10^{-6} \text{ W/m}^3$ , such that the surface temperature is  $0^\circ\text{C}$  and the temperature at the base of the model is  $600^\circ\text{C}$ . This geotherm remains in steady state when there is no material motion and is perturbed by material motion, such as rock uplift.

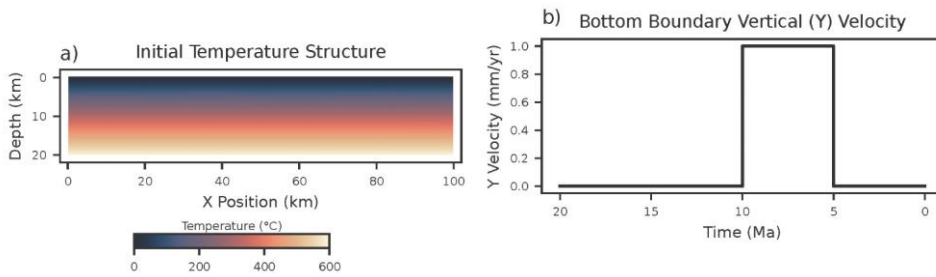


**Figure 4:** Initial conditions for simple model of exhumation within a 2D box. This box is assigned a linear geothermal gradient of  $30^\circ\text{C}$  with a surface temperature of  $0^\circ\text{C}$ . For 10 Myr, the box is kept static, such that the shallowest particles in or above the partial retention zones for AHe and ZHe and the partial annealing zone for AFT would accumulate He and fission tracks. Particles above) Model domain consisting of a  $100 \times 20 \text{ km}$  box of upper crust (density:  $2.8 \text{ g/cm}^3$ ; thermal conductivity:  $2.5 \text{ W/m} \cdot \text{K}$ ) with a conductive geothermal gradient defined by basal heat flow of  $85 \text{ mW/m}^2$  and radiogenic heating of  $1 \times 10^{-6} \text{ W/m}^3$ . b) Vertical velocity imposed on the bottom of the model during the model run over 20 Myr.

For 10 Myr (20-10 Ma), the box is kept static, so that particles in or shallower than the partial retention zones for AHe and ZHe and the partial annealing zone for AFT will accumulate He and fission tracks. Particles shallower than the partial retention/annealing zones will have ages of 10 Ma at this stage, particles within the partial retention/annealing zones will have ages between 0 and 10 Ma, and particles below deeper than the partial retention/annealing zones will have ages of 0 Ma. At 10 Myr, the bottom of the box is pushed upwards at a rate of  $1 \text{ mm/yr}$ , allowing material to exit through the top of the box while the temperature structure of the box remains constant and pushing isotherms upward as heat is advected. This is designed to simulate 5 km of rock uplift with perfectly efficient erosion maintaining the original surface of the model. Exhumation continues until 15 Myr, at which point the model remains static again until 20 Myr. This model is deliberately unrealistic and simplistic, with material advected upwards without deflecting isotherms variations in rock uplift or topography erosion rate, and is intended only as a benchmark to illustrate how temperatures from the results of geodynamic modeling software can be output to GDTchron to produce thermochronometric ages that would be expected in a highly controlled system.

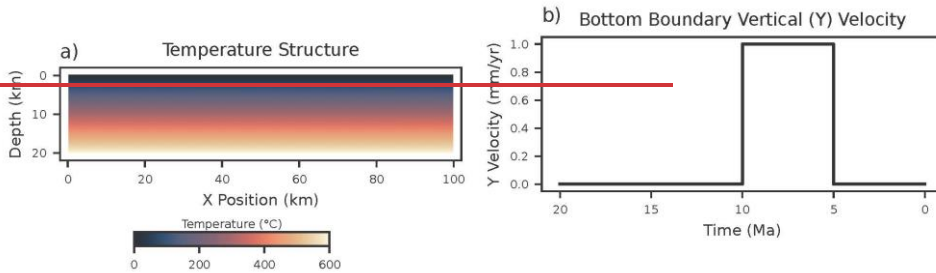


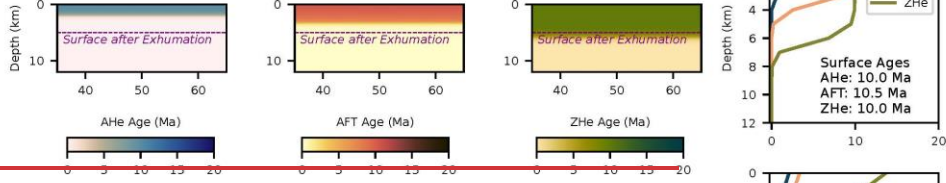
Figure 4: Initial conditions for simple model of exhumation within a 2D box. a) Model domain consisting of a 100 x 20 km box with a surface temperature of 0°C and a linear geothermal gradient of 30°C. b) Vertical velocity imposed on the bottom of the model during the model run over 20 Myr

Formatted: Normal

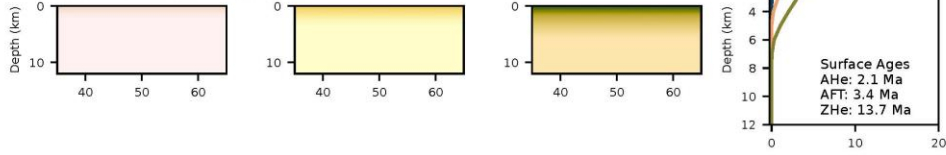
265 The output of this model consists of ~100,000 particles distributed over 200 timesteps of 100,000 years. Figure 5 shows the resulting AHe, AFT, and ZHe ages after post-processing this ASPECT output with GDTchron, using default values for U (100 ppm), Th (100 ppm), radius (50  $\mu\text{m}$ ), and  $D_{\text{par}}$  (1.75), which can be adjusted by the user. For each of these systems, during the first 10 Myr, (20-10 Ma), the shallowest particles begin with ages of 0 Ma and yield progressively older ages with time, with the ages at the surface of the model essentially equal to the model runtime. Ages young with depth through the partial retention/annealing zones of each thermochronometric system. At the base of these zones, ages are 0 Ma because diffusion and annealing outpace He and fission track production. During exhumation from 10 Myr/Ma to 15 Myr/5 Ma, the oldest ages at the surface are removed while material with younger ages is brought to the surface, smoothing the transition from young ages at depth to old ages at the surface. Surface AHe ages are the youngest, whereas ZHe ages are the oldest, reflecting the erosion of nearly the entire original AHe partial retention zone while much of the original ZHe partial zone remains intact.

275 During the final 5 Myr, (5-0 Ma), material near the surface gets progressively older again, resulting in final surface ages and age distributions at depth that are the cumulative effect of quiescence, exhumation, and additional quiescence.

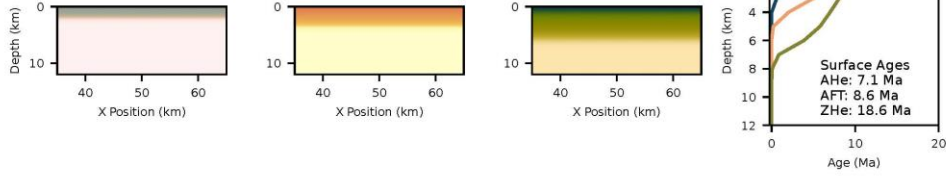
### 10 Ma - Before Exhumation



### 5 Ma - After Exhumation



### 0 Ma - After Quiescence



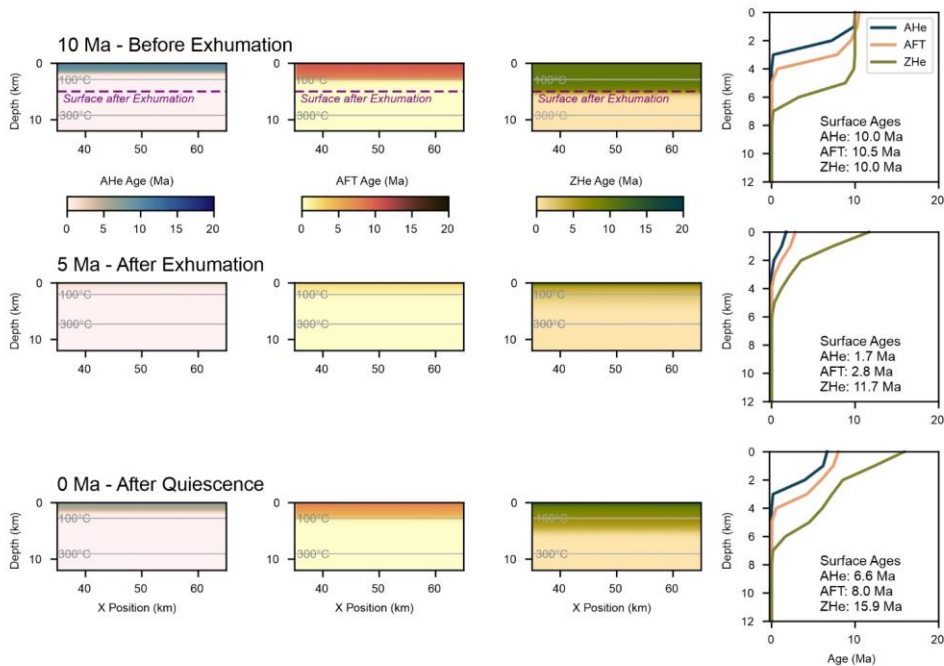


**Figure 5:** Results from 20 Myr model of simple exhumation for the apatite (U-Th)/He (AHe), apatite fission track (AFT), and zircon (U-Th)/He systems at key moments in the model run. Left three columns show distribution of ages for each of the three systems; right column shows age as a function of depth in the model domain, with age at the surface of the model reported. Grey contours show 100°C and 300°C isotherms. Top row (10 Ma) shows results after 10 Myr of ingrowth of He and fission tracks with no exhumation. Center row (5 Ma) shows results after 5 Myr of exhumation at 1 mm/yr, and bottom row (0 Ma) shows results after an additional 5 Myr of quiescence following exhumation.

285 This example model demonstrates the potential utility of our software as a means of assessing patterns of low-temperature thermochronometric age distribution in a variety of geodynamic settings. One could explore the effects of varying fault network evolution, surface processes, geothermal gradients, plate motions, and crustal rheology on expected age distribution and use real thermochronology data as a means of validating choices of model parameters.

#### 4 Application to complex geodynamic modeling of rift-inversion orogenesis

290 The exhumation model described above is deliberately simplistic in order to demonstrate expected patterns of thermochronometric ages in a highly controlled system. More complex geodynamic models can deploy realistic deformation,

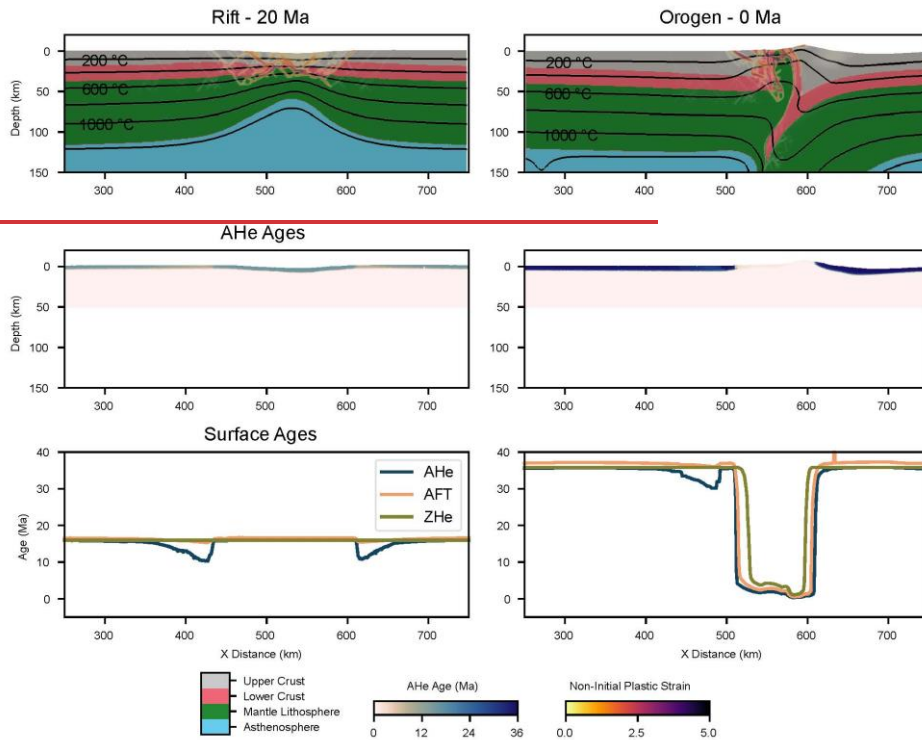
geothermal gradients, surface processes, mantle convection, radiogenic heat production, shear heating, and other features that impact the thermal history material within the model. Since all these processes can impact the final ages derived from rocks at the surface of the Earth, these models provide a means of testing the sensitivity of ages to variations within these parameters and of using patterns of ages from natural settings to validate geodynamic models.

To demonstrate one of many possible examples, Figure 6 shows the results of processing an ASPECT model of rift-inversion orogenesis with GDTchron to generate synthetic AHe, AFT, and ZHe ages. Rift-inversion orogens are compressional mountain belts in which a continental rift present prior to compression serves as a preexisting lithospheric weakness that localizes deformation (e.g., Cooper et al., 1989; Vasey et al., 2024; Zwaan et al., 2025)(e.g., Cooper et al., 1989; Vasey et al., 2024; Zwaan et al., 2025). These orogens, which include the Pyrenees (e.g., Muñoz, 1992)(e.g., Muñoz, 1992), High Atlas (e.g., Beauchamp et al., 1999), and Greater Caucasus (e.g., Vincent et al., 2016) have multi-phase thermal histories that may include periods of extension, tectonic quiescence, and compression, all of which may impact the final thermochronometric ages recorded in rocks exposed within the present-day mountain belt. Thus, predicting synthetic ages within models of rift-inversion orogenesis serves as a means of deconvolving the impacts of the individual phases on the final thermal imprint recorded by thermochronology.

Unlike the model presented above (Figure 5), in which rock uplift, and erosion, and geothermal gradient are highly prescribed, this geodynamic model employs more realistic approximations of these key parameters (Vasey et al., 2024). Deformation is driven by horizontal velocities imposed on the model sides, with rock uplift resulting from the response of crust and mantle materials to the imposed deviatoric stresses. A Drucker-Prager yield criterion with a plastic damper serves as an approximation of brittle deformation in this model (Duretz et al., 2020), and flow laws for dislocation and/or diffusion creep govern viscous flow (Gleason and Tullis, 1995; Hirth and Kohlstedt, 2003; Rybaeki et al., 2006)(Gleason and Tullis, 1995; Hirth and Kohlstedt, 2003; Rybaeki et al., 2006). Strain weakening is implemented by reducing the angle of internal friction and cohesion as a function of accumulated strain. Erosion is simulated by the surface processes code FastScape, which uses a combination of hillslope diffusion, the stream power law, and marine transport/deposition to modify the free surface in response to surface uplift (Braun and Willett, 2013; Neuharth et al., 2022; Yuan et al., 2019a, b). The initial geothermal gradient blends a conductive cooling profile within the lithosphere (Chapman, 1986) with an approximated adiabatic temperature profile that dominates temperature gradients in the convecting mantle. Temperature evolution is modeled with a combination of advection, heat conduction, radiogenic heating, shear heating, and adiabatic heating.

Thermokinematic models like Pecube (Braun, 2003; Braun et al., 2012) and Pecube-D (Ehlers, 2023)(Ehlers, 2023) have often been used to predict thermochronometric ages in rift-inversion orogens (e.g., Capaldi et al., 2022; Curry et al., 2021; Erdős et al., 2014)(e.g., Capaldi et al., 2022; Curry et al., 2021; Erdős et al., 2014). Such models do an excellent job of predicting ages when using prescribed motions derived from regional data in conjunction with models of topographic evolution, but they are

unable to simulate the dynamic surface response of deforming lithosphere to far-field plate motions. We are only aware of one prior study focused on the Pyrenees (Ternois et al., 2021) in which fully dynamic models of rift-inversion orogens were used to predict thermochronometric ages. This study extracted the thermal history of only 14 tracer particles, which were then manually passed to the software QTQt (Gallagher, 2012) for forward modeling.



330

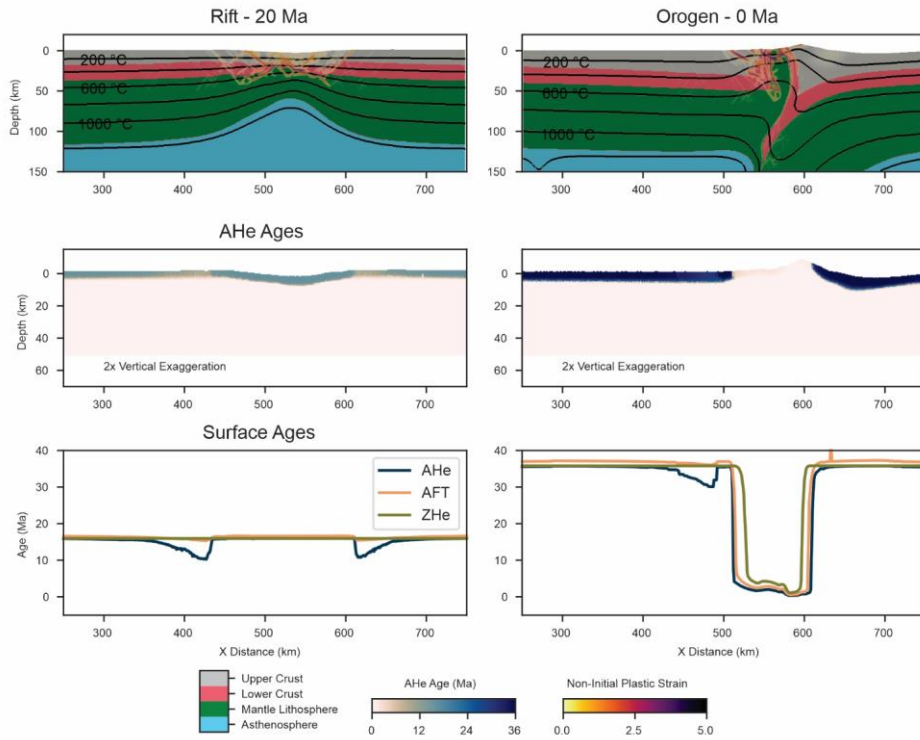


**Figure 6:** Results from 36 Myr rift inversion model at the rift (left column, 20 Ma) and the inversion stage (right column, 0 Ma), designed after Model 1 in Vasey et al. (2024) with the addition of surface processes from the code FastScape. Top row shows distribution of compositional layers, plastic strain, and temperature structure. Middle row shows distribution of apatite (U-Th)/He (AHe) ages for the [same view upper 50 km](#) of the model domain so that ages can be directly compared with the top row. Bottom row shows AHe, apatite fission track (AFT), and zircon (U-Th)/He ages at the surface along the X component of the model domain.

Our example model is based on Model 1 from Vasey et al. (2024) but is modified to provide more realistic surface processes through coupling of ASPECT with the surface processes code FastScape (Braun and Willett, 2013; Neuharth et al., 2022; Yuan et al., 2019a, b). The models in Vasey et al. (2024) [used](#) hillslope diffusion to approximate surface processes (Sandiford et al., 2021), and we [found](#) that such diffusion [dampened](#) exhumation sufficiently to prevent exposure of material with young thermochronometric ages at the surface of the model. This discrepancy highlights that the choice of surface processes model and associated parameters is critical to meaningful prediction of thermochronometric ages in geodynamic models (e.g., Gilmore et al., 2018; Ketcham, 2025) (e.g., Gilmore et al., 2018; Ketcham, 2025), since such choices could result

in erroneously young ages if erosion is too efficient or in erroneously old ages if erosion is too inefficient. We note that  
345 GDTchron presents an opportunity for modelers to use thermochronometric age prediction as a means of testing their surface  
processes implementations; if surface age patterns are unrealistic compared to natural examples, it may highlight unrealistic  
topographic evolution that could also be influencing other components of the model results.

Both the Vasey et al. (2024) model and the model presented here simulate rift inversion over a total model runtime of 36 Myr  
350 by first extending a 1000 x 600 km block divided into upper crust, lower crust, mantle lithosphere, and asthenosphere for 16  
Myr (36-20 Ma) at 0.5 cm/yr to create a continental rift. After 16 Myr (20 Ma), the model then undergoes convergence at 1  
cm/yr for 20 Myr (20-0 Ma) to invert the rift and create a mountain belt. These specific model parameters result in an  
asymmetric mountain belt, with the lithosphere on one side of the model underthrust beneath the lithosphere on the other side,  
and development of major shear zones approximating the orogenic wedge of a real mountain belt (e.g., Beaumont et al., 1996;  
355 Dahlen, 1984; Willett et al., 1993).

During rifting, the flanks of the rift are uplifted and exhumed relative to the down-dropping basin, resulting in slightly younger  
AHe (~10 Ma) and AFT (~14 Ma) ages at the surface of the rift flanks relative to elsewhere along the surface after 16 Myr (20  
360 Ma) due to partial resetting of these thermochronometric systems. Insufficient material is exhumed to reset ZHe ages, given  
the deeper partial retention zone of this system (e.g., Reiners and Brandon, 2006). During rift inversion, rapid exhumation in  
the center of the model occurs due to lithospheric thickening, rock uplift, and erosion, leading to a zone of young (<5 Ma)  
AHe, AFT, and ZHe ages at the end of orogenesis. Notably, this zone widens as deformation propagates towards the forelands  
on either side of the doubly-vergent ~~orogenic wedge~~ orogen, overprinting the rift flank signal on the right (prowedge) side of  
the model. On the left (retrowedge) side of the model, the effects of rifting are preserved as a zone of slightly younger AHe  
365 (~30 Ma) and AFT (~35 Ma) ages. Because our software allows us to see the evolution of these thermochronometric systems  
throughout the model run, it is possible to clearly separate the effects of rifting and inversion. Modifying the parameters of rift  
inversion to change the structure of the rift and orogen will likely also change the patterns of thermochronometric ages, which  
can then be compared to the increasing quantity of observational data from rift-inversion orogens like the Pyrenees (e.g., Curry  
et al., 2021), High Atlas (e.g., Lanari et al., 2020), and Greater Caucasus (e.g., Vincent et al., 2020).

## 370 5 Limitations and future directions

We emphasize that the current version of our software represents only the first step towards more fruitful combination of  
geodynamic modeling with low-temperature thermochronology. Currently, the software only employs a simple He diffusion  
model for AHe (Farley, 2000) and ZHe (Reiners et al., 2004), whereas considerable work has gone into developing models  
that take radiation damage and annealing into account (e.g., Enkelmann and Garver, 2016; Flowers et al., 2009; Guenther,  
375 2021; Guenther et al., 2013, 2014; Shuster et al., 2006). Likewise, only the model of Ketchum et al. (1999) for fission track

annealing in the AFT system is currently used, and numerous improvements in modeling annealing have been proposed since that time (e.g., Ketcham, 2019; Ketcham et al., 2007; Tamer and Ketcham, 2020)(e.g., Ketcham, 2019; Ketcham et al., 2007; Tamer and Ketcham, 2020), and models of the zircon fission track (ZFT) system could also be implemented (e.g., Yamada et al., 2007). Our current software also does not allow for U-Th zonation (e.g., Ault and Flowers, 2012; Farley et al., 2011; Hourigan et al., 2005) or geometries other than a sphere (e.g., Glotzbach et al., 2019; Herman et al., 2007) when modeling He diffusion. Implementing these alternative kinetic models in future versions would allow one to see if and how these choices would affect the large-scale distribution of ages within a particular geodynamic setting.

Importantly, the ages produced when applying outputs from geodynamic models are dependent on parameters that would be highly variable among samples within real systems (e.g., U and Th concentrations, grain size,  $D_{\text{par}}$ ), creating a certain level of arbitrariness that must be taken into account when comparing model results with data from natural systems. However, we note that the choices of these parameters are no less arbitrary than many of the choices widely adopted for other parameters in geodynamic models, such as the common choice to use an experimentally-derived viscous flow law for quartz aggregates (Gleason and Tullis, 1995) to model the rheology of the entire upper crust. GDTchron currently applies single values for U and Th concentrations, grain size, and  $D_{\text{par}}$  for the entire model domain, though the user can adjust these values to assess the impact of these parameters on the predicted ages.

Other limitations of our software as currently implemented derive from the nature of the geodynamic models used as inputs. Real thermochronometric ages contain additional thermal inheritance that is difficult to capture within such models. In particular, sedimentary rocks frequently contain detrital apatite and zircon grains that reflect the thermal history of the source rocks that were eroded (e.g., Malusà and Fitzgerald, 2020; Rahl et al., 2007), and mimicking this process accurately in a geodynamic model requires not only simulating erosion and deposition but also tracking where eroded material is deposited. In the example rift inversion model above, such tracking does not take place, and since new sediment has no inherited thermal history, it is simply assigned the thermal history of the material upon which it is deposited via interpolation (Figure 6). Enabling such tracking within ASPECT and/or other geodynamic modeling codes would enhance the ability of our software to simulate the detrital component of thermochronology. This would require either allowing new sediment to inherit the unique particle ID assigned to its source material or the creation of a new field that connects sediment to its source material so that GDTchron could transfer the relevant thermal history.

Finally, although designing GDTchron as a Python package has the advantage of making it open-source, readable, and flexible, that comes with a tradeoff in performance relative to compiled programming languages like C++ and Fortran (e.g., Cai et al., 2005). Although we have aimed to optimize GDTchron where possible by vectorizing calculations and using sparse matrices, additional performance improvements could be implemented in future versions. Additionally, the current parallelized workflow using Joblib currently limits calculations to a single node on an HPC cluster, and larger parallel computations across

410 multiple nodes could be achieved using tools like Dask (Rocklin, 2015) or mpi4py (Dalcin and Fang, 2021). Such improvements would enable GDTchron to be used more efficiently for large high-resolution and/or 3D geodynamic models.

By providing an open-source version of our code on GitHub that is carefully annotated and paired with interactive examples in Jupyter Notebooks, we hope to encourage community development that will address these and other limitations of the existing software. Recent efforts to gather large compilations of thermochronologic data (e.g., Boone et al., 2023; Lanari et al., 2023)(e.g., Boone et al., 2023; Lanari et al., 2023) provide ample opportunity for geodynamic modelers to compare their results with observations. Our intention is for this software to be a tool that can grow as needed to fit the needs of both the geodynamic and thermochronology communities for research and training purposes. Our GitHub repository contains instructions for how to use the code as well as how to make contributions, and we welcome new collaborations for future versions.

## 6 Conclusions

We present GDTchron: an open-source Python package designed to forward model large numbers of thermochronometric ages from the time-temperature (t-T) paths output by geodynamic numerical models. GDTchron adopts previously used modeling approaches and kinetic parameters to estimate apatite (U-Th)/He (AHe), apatite fission track (AFT), and zircon (U-Th)/He (ZHe) ages in a parallelized workflow that can take advantage of multi-core processors and high-performance computing (HPC) nodes. The package can extract t-T paths for unique particles from commonly used output file formats in geodynamic modeling and estimate ages for all parts of the model domain throughout the model run. An interpolation scheme using  $k$ -d trees allows particles created during the model run to inherit the thermal histories and ages of their nearest neighbors. A simple model of exhumation and a more complex model of rift-inversion orogenesis illustrate potential use-cases for this package.

430 The code is designed to facilitate development by the community as needed for improved functionality.

## Author Contributions

DV and PS wrote the Python code. DV, PS, JN, and SB designed and ran the geodynamic models in ASPECT. DV wrote the initial draft, and all authors contributed to revision and preparation of subsequent drafts.

## Code/Data Availability

435 The source code for the Python package, Jupyter Notebooks used for analysis and figures, and ASPECT parameter files for the geodynamic models are all available in a GitHub repository (<https://github.com/dyvasey/gdtchron>), which is also archived at Zenodo (Vasey and Seully, 2025)(Vasey et al., 2026). The files in this repository allow the exhumation model to be

reproduced in its entirety on a personal computer, and the rift inversion model could also be replicated with an ASPECT installation on an HPC cluster. The Jupyter Notebooks include videos showing the full evolution of the exhumation and rift inversion models. GDTchron can be installed in a Python environment from the GitHub repository or from the package repositories PyPI and conda-forge.

### Competing Interests

The authors declare that they have no conflict of interest.

### Acknowledgements

445 Financial support for this study was provided to D. Vasey by Tufts University, with scaling tests and ASPECT model runs conducted on the Tufts High Performance Compute (HPC) Cluster (<https://it.tufts.edu/high-performance-computing>). We thank the Computational Infrastructure for Geodynamics (<https://geodynamics.org>), which is funded by the National Science Foundation under awards EAR-0949446, EAR-1550901, and EAR-2149126, for supporting the development of ASPECT. S. Brune was funded by the European Union (ERC, EMERGE, 101087245). We thank Chelsea Mackaman-Lofland and Kendra Murray for constructive reviews that greatly improved the quality of the manuscript, as well as Associate Editor Shigeru Sueoka for editorial handling. We thank Anne Glerum and Frank Zwaan for their contributions to the rift inversion model used as an example application of GDTchron. We also thank Jim McClain for early conversations with D. Vasey that contributed to the idea for GDTchron.

### References

- 455 Almendral, A., Robles, W., Parra, M., Mora, A., Ketcham, R. A., and Raghil, M.: FetKin: Coupling kinematic restorations and temperature to predict thrusting, exhumation histories, and thermochronometric ages, *AAPG Bulletin*, 99, 1557–1573, <https://doi.org/10.1306/07071411112>, 2015.
- Ault, A. K. and Flowers, R. M.: Is apatite U–Th zonation information necessary for accurate interpretation of apatite (U–Th)/He thermochronometry data?, *Geochimica et Cosmochimica Acta*, 79, 60–78, <https://doi.org/10.1016/j.gca.2011.11.037>, 2012.
- 460 Balázs, A., Faccenna, C., Ueda, K., Funicello, F., Boutoux, A., Blanc, E. J.-P., and Gerya, T.: Oblique subduction and mantle flow control on upper plate deformation: 3D geodynamic modeling, *Earth and Planetary Science Letters*, 569, 117056, <https://doi.org/10.1016/j.epsl.2021.117056>, 2021.
- Bangerth, W., Dannberg, J., Fraters, M., Gassmoeller, R., Glerum, A., Heister, T., Myhill, R., and Naliboff, J.: ASPECT v3.0.0, 2024.

- Beauchamp, W., Allmendinger, R. W., Barazangi, M., Demnati, A., Alji, M. E., and Dahmani, M.: Inversion tectonics and the evolution of the High Atlas Mountains, Morocco, based on a geological-geophysical transect, *Tectonics*, 18, 163–184, <https://doi.org/10.1029/1998TC900015>, 1999.
- 470 Beaumont, C., Ellis, S., Hamilton, J., and Fullsack, P.: Mechanical model for subduction-collision tectonics of Alpine-type  
compressional orogens, *Geology*, 24, 675–678, [https://doi.org/10.1130/0091-7613\(1996\)024%253C06753C0675::MMFSC%253E23E2.3.CO;2](https://doi.org/10.1130/0091-7613(1996)024%253C06753C0675::MMFSC%253E23E2.3.CO;2), 1996.
- van der Beek, P. and Schildgen, T. F.: Short communication: *age2exhume* – a MATLAB/Python script to calculate steady-state vertical exhumation rates from thermochronometric ages and application to the Himalaya, *Geochronology*, 5, 35–49, <https://doi.org/10.5194/gchron-5-35-2023>, 2023.
- 475 Bentley, J. L.: Multidimensional binary search trees used for associative searching, *Commun. ACM*, 18, 509–517, <https://doi.org/10.1145/361002.361007>, 1975.
- Boone, S. C., Kohlmann, F., Noble, W., Theile, M., Beucher, R., Kohn, B., Glorie, S., Danišik, M., Zhou, R., McMillan, M., Nixon, A., Gleadow, A., Qin, X., Müller, D., and McInnes, B.: A geospatial platform for the tectonic interpretation of low-temperature thermochronology Big Data, *Sci Rep*, 13, 8581, <https://doi.org/10.1038/s41598-023-35776-3>, 2023.
- 480 Braun, J.: Pecube: a new finite-element code to solve the 3D heat transport equation including the effects of a time-varying, finite amplitude surface topography, *Computers & Geosciences*, 29, 787–794, [https://doi.org/10.1016/S0098-3004\(03\)00052-9](https://doi.org/10.1016/S0098-3004(03)00052-9), 2003.
- Braun, J. and Willett, S. D.: A very efficient O(n), implicit and parallel method to solve the stream power equation governing fluvial incision and landscape evolution, *Geomorphology*, 180–181, 170–179, <https://doi.org/10.1016/j.geomorph.2012.10.008>, 2013.
- 485 Braun, J., van der Beek, P., Valla, P., Robert, X., Herman, F., Glotzbach, C., Pedersen, V., Perry, C., Simon-Labric, T., and Prigent, C.: Quantifying rates of landscape evolution and tectonic processes by thermochronology and numerical modeling of crustal heat transport using PECUBE, *Tectonophysics*, 524–525, 1–28, <https://doi.org/10.1016/j.tecto.2011.12.035>, 2012.
- Burkett, E. R. and Billen, M. I.: Dynamics and implications of slab detachment due to ridge-trench collision, *Journal of Geophysical Research: Solid Earth*, 114, <https://doi.org/10.1029/2009JB006402>, 2009.
- 490 Cai, X., Langtangen, H. P., and Moe, H.: On the Performance of the Python Programming Language for Serial and Parallel Scientific Computations, *Scientific Programming*, 13, 619804, <https://doi.org/10.1155/2005/619804>, 2005.
- Capaldi, T. N., Odium, M. L., Curry, M. E., and Stockli, D. F.: Variable thermal histories across the Pyrenees orogen recorded in modern river sand detrital geo-/thermochronology and PECUBE thermokinematic modelling, *Basin Research*, 34, 1781–1806, <https://doi.org/10.1111/bre.12685>, 2022.
- 495 [Chapman, D. S.: Thermal gradients in the continental crust, Geological Society, London, Special Publications, 24, 63–70, https://doi.org/10.1144/GSL.SP.1986.024.01.07, 1986.](https://doi.org/10.1144/GSL.SP.1986.024.01.07)
- Coltice, N., Husson, L., Faccenna, C., and Arnould, M.: What drives tectonic plates?, *Science Advances*, 5, eaax4295, <https://doi.org/10.1126/sciadv.aax4295>, 2019.
- 500 Cooper, M. A., Williams, G. D., Graciansky, P. C. de, Murphy, R. W., Needham, T., Paor, D. de, Stoneley, R., Todd, S. P., Turner, J. P., and Ziegler, P. A.: Inversion tectonics - A discussion, *Geological Society, London, Special Publications*, 44, 335–347, <https://doi.org/10.1144/GSL.SP.1989.044.01.18>, 1989.

- Cramer, F., Shephard, G. E., and Heron, P. J.: The misuse of colour in science communication, *Nat Commun*, 11, 5444, <https://doi.org/10.1038/s41467-020-19160-7>, 2020.
- 505 Curry, M. E., Beek, P. van der, Huisman, R. S., Wolf, S. G., Fillon, C., and Muñoz, J.-A.: Spatio-temporal patterns of Pyrenean exhumation revealed by inverse thermo-kinematic modeling of a large thermochronologic data set, *Geology*, 49, 738–742, <https://doi.org/10.1130/G48687.1>, 2021.
- Dahlen, F. A.: Noncohesive critical Coulomb wedges: An exact solution, *Journal of Geophysical Research: Solid Earth*, 89, 10125–10133, <https://doi.org/10.1029/JB089iB12p10125>, 1984.
- 510 Dalcin, L. and Fang, Y.-L. L.: mpi4py: Status Update After 12 Years of Development, *Computing in Science & Engineering*, 23, 47–54, <https://doi.org/10.1109/MCSE.2021.3083216>, 2021.
- Duretz, T., Gerya, T. V., and May, D. A.: Numerical modelling of spontaneous slab breakoff and subsequent topographic response, *Tectonophysics*, 502, 244–256, <https://doi.org/10.1016/j.tecto.2010.05.024>, 2011.
- 515 Duretz, T., de Borst, R., Yamato, P., and Le Pourhiet, L.: Toward Robust and Predictive Geodynamic Modeling: The Way Forward in Frictional Plasticity, *Geophysical Research Letters*, 47, e2019GL086027, <https://doi.org/10.1029/2019GL086027>, 2020.
- Ehlers, T. A.: Pecube-D: Thermokinematic and Erosion Modeling Software for problems in Tectonics and Surface Processes, <https://doi.org/10.5281/zenodo.7785668>, 2023.
- 520 Enkelmann, E. and Garver, J. I.: Low-temperature thermochronology applied to ancient settings, *Journal of Geodynamics*, 93, 17–30, <https://doi.org/10.1016/j.jog.2015.11.001>, 2016.
- Erdős, Z., van der Beek, P., and Huisman, R. S.: Evaluating balanced section restoration with thermochronology data: A case study from the Central Pyrenees, *Tectonics*, 33, 617–634, <https://doi.org/10.1002/2013TC003481>, 2014.
- Farley, K. A.: Helium diffusion from apatite: General behavior as illustrated by Durango fluorapatite, *Journal of Geophysical Research*, 105, 2903–2914, 2000.
- 525 Farley, K. A., Shuster, D. L., and Ketcham, R. A.: U and Th zonation in apatite observed by laser ablation ICPMS, and implications for the (U–Th)/He system, *Geochimica et Cosmochimica Acta*, 75, 4515–4530, <https://doi.org/10.1016/j.gca.2011.05.020>, 2011.
- Flowers, R. M. and Peak, B. A.: Context matters: Modeling thermochronologic data in geologic frameworks using the Great Unconformity as a case study, *Earth and Planetary Science Letters*, 650, 119061, <https://doi.org/10.1016/j.epsl.2024.119061>, 530 2025.
- Flowers, R. M., Ketcham, R. A., Shuster, D. L., and Farley, K. A.: Apatite (U–Th)/He thermochronometry using a radiation damage accumulation and annealing model, *Geochimica et Cosmochimica Acta*, 73, 2347–2365, <https://doi.org/10.1016/j.gca.2009.01.015>, 2009.
- 535 Flowers, R. M., Zeitler, P. K., Danišik, M., Reiners, P. W., Gautheron, C., Ketcham, R. A., Metcalf, J. R., Stockli, D. F., Enkelmann, E., and Brown, R. W.: (U–Th)/He chronology: Part 1. Data, uncertainty, and reporting, *GSA Bulletin*, 135, 104–136, <https://doi.org/10.1130/B36266.1>, 2023a.

Flowers, R. M., Ketcham, R. A., Enkelmann, E., Gautheron, C., Reiners, P. W., Metcalf, J. R., Danišik, M., Stockli, D. F., and Brown, R. W.: (U-Th)/He chronology: Part 2. Considerations for evaluating, integrating, and interpreting conventional individual aliquot data, *GSA Bulletin*, 135, 137–161, <https://doi.org/10.1130/B36268.1>, 2023b.

540 Fosdick, J. C., Stevens Goddard, A. L., Mackaman-Lofland, C., Lossada, A. C., Rodríguez, M. P., and Carrapa, B.: Eocene exhumation of the High Andes at ~30°S differentiated by detrital multimethod U-Pb-He thermochronology, *Geology*, 52, 678–682, <https://doi.org/10.1130/G52272.1>, 2024.

545 Fraters, M. R. T. and Billen, M. I.: On the Implementation and Usability of Crystal Preferred Orientation Evolution in Geodynamic Modeling, *Geochemistry, Geophysics, Geosystems*, 22, e2021GC009846, <https://doi.org/10.1029/2021GC009846>, 2021.

Gallagher, K.: Transdimensional inverse thermal history modeling for quantitative thermochronology, *J. Geophys. Res.*, 117, B02408, <https://doi.org/10.1029/2011JB008825>, 2012.

Gallagher, K. and Parra, M.: A new approach to thermal history modelling with detrital low temperature thermochronological data, *Earth and Planetary Science Letters*, 529, 115872, <https://doi.org/10.1016/j.epsl.2019.115872>, 2020.

550 Gassmöller, R., Lokavarapu, H., Heien, E., Puckett, E. G., and Bangerth, W.: Flexible and Scalable Particle-in-Cell Methods with Adaptive Mesh Refinement for Geodynamic Computations, *Geochemistry, Geophysics, Geosystems*, 19, 3596–3604, <https://doi.org/10.1029/2018GC007508>, 2018.

555 Gassmöller, R., Lokavarapu, H., Bangerth, W., and Puckett, E. G.: Evaluating the accuracy of hybrid finite element/particle-in-cell methods for modelling incompressible Stokes flow, *Geophysical Journal International*, 219, 1915–1938, <https://doi.org/10.1093/gji/ggz405>, 2019.

Gilmore, M. E., McQuarrie, N., Eizenhöfer, P. R., and Ehlers, T. A.: Testing the effects of topography, geometry, and kinematics on modeled thermochronometer cooling ages in the eastern Bhutan Himalaya, *Solid Earth*, 9, 599–627, <https://doi.org/10.5194/se-9-599-2018>, 2018.

560 Gleason, G. C. and Tullis, J.: A flow law for dislocation creep of quartz aggregates determined with the molten salt cell, *Tectonophysics*, 247, 1–23, [https://doi.org/10.1016/0040-1951\(95\)00011-B](https://doi.org/10.1016/0040-1951(95)00011-B), 1995.

Glerum, A. C., Brune, S., Magnall, J. M., Weis, P., and Gleeson, S. A.: Geodynamic controls on clastic-dominated base metal deposits, *Solid Earth*, 15, 921–944, <https://doi.org/10.5194/se-15-921-2024>, 2024.

Glotzbach, C., Lang, K. A., Avdievitch, N. N., and Ehlers, T. A.: Increasing the accuracy of (U-Th(-Sm))/He dating with 3D grain modelling, *Chemical Geology*, 506, 113–125, <https://doi.org/10.1016/j.chemgeo.2018.12.032>, 2019.

565 Guenther, W. R.: Implementation of an Alpha Damage Annealing Model for Zircon (U-Th)/He Thermochronology With Comparison to a Zircon Fission Track Annealing Model, *Geochemistry, Geophysics, Geosystems*, 22, e2019GC008757, <https://doi.org/10.1029/2019GC008757>, 2021.

570 Guenther, W. R., Reiners, P. W., Ketcham, R. A., Nasdala, L., and Giester, G.: Helium diffusion in natural zircon: Radiation damage, anisotropy, and the interpretation of zircon (U-Th)/He thermochronology, *Am J Sci*, 313, 145–198, <https://doi.org/10.2475/03.2013.01>, 2013.

Guenther, W. R., Reiners, P. W., and Tian, Y.: Interpreting date–eU correlations in zircon (U-Th)/He datasets: A case study from the Longmen Shan, China, *Earth and Planetary Science Letters*, 403, 328–339, <https://doi.org/10.1016/j.epsl.2014.06.050>, 2014.

- 575 Heister, T., Dannberg, J., Gasmöller, R., and Bangerth, W.: High accuracy mantle convection simulation through modern numerical methods – II: realistic models and problems, *Geophysical Journal International*, 210, 833–851, <https://doi.org/10.1093/gji/ggx195>, 2017.
- Herman, F., Braun, J., Senden, T. J., and Dunlap, W. J.: (U–Th)/He thermochronometry: Mapping 3D geometry using micro-X-ray tomography and solving the associated production–diffusion equation, *Chemical Geology*, 242, 126–136, <https://doi.org/10.1016/j.chemgeo.2007.03.009>, 2007.
- 580 Hirth, G. and Kohlstedt, D.: Rheology of the upper mantle and the mantle wedge: A view from the experimentalists, *Geophysical Monograph-American Geophysical Union*, 138, 83–106, 2003.
- Hourigan, J. K., Reiners, P. W., and Brandon, M. T.: U-Th zonation-dependent alpha-ejection in (U-Th)/He chronometry, *Geochimica et Cosmochimica Acta*, 69, 3349–3365, <https://doi.org/10.1016/j.gca.2005.01.024>, 2005.
- 585 Jourdon, A. and May, D. A.: An efficient partial-differential-equation-based method to compute pressure boundary conditions in regional geodynamic models, *Solid Earth*, 13, 1107–1125, <https://doi.org/10.5194/se-13-1107-2022>, 2022.
- Jourdon, A., Le Pourhiet, L., Petit, C., and Rolland, Y.: The deep structure and reactivation of the Kyrgyz Tien Shan: Modelling the past to better constrain the present, *Tectonophysics*, 746, 530–548, <https://doi.org/10.1016/j.tecto.2017.07.019>, 2018.
- Kaus, B. J., Popov, A. A., Baumann, T., Pusok, A., Bauville, A., Fernandez, N., and Collignon, M.: Forward and inverse modelling of lithospheric deformation on geological timescales, *Proceedings of nic symposium*, 978–983, 2016.
- 590 Ketcham, R., Donelick, R., and Donelick, M.: AFT solve: A program for multi-kinetic modeling of apatite fission track data: *Geological Material Research*, 2000.
- Ketcham, R. A.: Forward and inverse modeling of low-temperature thermochronometry data, *Reviews in Mineralogy and Geochemistry*, 58, 275–314, <https://doi.org/10.2138/rmg.2005.58.11>, 2005.
- 595 Ketcham, R. A.: Fission-Track Annealing: From Geologic Observations to Thermal History Modeling, in: *Fission-Track Thermochronology and its Application to Geology*, edited by: Malusà, M. G. and Fitzgerald, P. G., Springer International Publishing, Cham, 49–75, [https://doi.org/10.1007/978-3-319-89421-8\\_3](https://doi.org/10.1007/978-3-319-89421-8_3), 2019.
- Ketcham, R. A.: Thermal history inversion from thermochronometric data and complementary information: New methods and recommended practices, *Chemical Geology*, 653, 122042, <https://doi.org/10.1016/j.chemgeo.2024.122042>, 2024.
- 600 Ketcham, R. A.: Technical note: Incorporating topographic deflection effects into thermal history modelling, *Geochronology*, 7, 449–458, <https://doi.org/10.5194/gchron-7-449-2025>, 2025.
- Ketcham, R. A., Donelick, R. A., and Carlson, W. D.: Variability of apatite fission-track annealing kinetics: III. Extrapolation to geological time scales, *American Mineralogist*, 84, 1235–1255, <https://doi.org/10.2138/am-1999-0903>, 1999.
- Ketcham, R. A., Carter, A., Donelick, R. A., Barbarand, J., and Hurford, A. J.: Improved modeling of fission-track annealing in apatite, *American Mineralogist*, 92, 799–810, <https://doi.org/10.2138/am.2007.2281>, 2007.
- 605 Ketcham, R. A., Gautheron, C., and Tassan-Got, L.: Accounting for long alpha-particle stopping distances in (U–Th–Sm)/He geochronology: Refinement of the baseline case, *Geochimica et Cosmochimica Acta*, 75, 7779–7791, <https://doi.org/10.1016/j.gca.2011.10.011>, 2011.

- Kronbichler, M., Heister, T., and Bangerth, W.: High accuracy mantle convection simulation through modern numerical methods, *Geophysical Journal International*, 191, 12–29, <https://doi.org/10.1111/j.1365-246X.2012.05609.x>, 2012.
- 610 Lanari, R., Fellin, M. G., Faccenna, C., Balestrieri, M. L., Pazzaglia, F. J., Youbi, N., and Maden, C.: Exhumation and surface evolution of the Western High Atlas and surrounding regions as constrained by low-temperature thermochronology, *Tectonics*, 39, e2019TC005562, <https://doi.org/10.1029/2019TC005562>, 2020.
- Lanari, R., Boutoux, A., Faccenna, C., Herman, F., Willett, S. D., and Ballato, P.: Cenozoic exhumation in the Mediterranean and the Middle East, *Earth-Science Reviews*, 237, 104328, <https://doi.org/10.1016/j.earscirev.2023.104328>, 2023.
- 615 [Lock, J. and Willett, S.: Low-temperature thermochronometric ages in fold-and-thrust belts, \*Tectonophysics\*, 456, 147–162, <https://doi.org/10.1016/j.tecto.2008.03.007>, 2008.](#)
- Malusà, M. G. and Fitzgerald, P. G.: The geologic interpretation of the detrital thermochronology record within a stratigraphic framework, with examples from the European Alps, Taiwan and the Himalayas, *Earth-Science Reviews*, 201, 103074, <https://doi.org/10.1016/j.earscirev.2019.103074>, 2020.
- 620 May, D. A., Brown, J., and Pourhiet, L. L.: pTatin3D: High-Performance Methods for Long-Term Lithospheric Dynamics, in: SC '14: Proceedings of the International Conference for High Performance Computing, Networking, Storage and Analysis, 274–284, <https://doi.org/10.1109/SC.2014.28>, 2014.
- Muñoz, J. A.: Evolution of a continental collision belt: ECORS-Pyrenees crustal balanced cross-section, in: *Thrust Tectonics*, edited by: McClay, K. R., Springer Netherlands, Dordrecht, 235–246, [https://doi.org/10.1007/978-94-011-3066-0\\_21](https://doi.org/10.1007/978-94-011-3066-0_21), 1992.
- 625 Neuharth, D., Brune, S., Wrona, T., Glerum, A., Braun, J., and Yuan, X.: Evolution of Rift Systems and Their Fault Networks in Response to Surface Processes, *Tectonics*, 41, e2021TC007166, <https://doi.org/10.1029/2021TC007166>, 2022.
- Rahl, J. M., Ehlers, T. A., and van der Pluijm, B. A.: Quantifying transient erosion of orogens with detrital thermochronology from syntectonic basin deposits, *Earth and Planetary Science Letters*, 256, 147–161, <https://doi.org/10.1016/j.epsl.2007.01.020>, 2007.
- 630 Reiners, P. W. and Brandon, M. T.: Using thermochronology to understand orogenic erosion, *Annu. Rev. Earth Planet. Sci.*, 34, 419–466, 2006.
- Reiners, P. W., Spell, T. L., Nicolescu, S., and Zanetti, K. A.: Zircon (U-Th)/He thermochronometry: He diffusion and comparisons with <sup>40</sup>Ar/<sup>39</sup>Ar dating, *Geochimica et Cosmochimica Acta*, 68, 1857–1887, <https://doi.org/10.1016/j.gca.2003.10.021>, 2004.
- 635 [Reiners, P. W., Ehlers, T. A., and Zeitler, P. K.: Past, Present, and Future of Thermochronology, \*Reviews in Mineralogy and Geochemistry\*, 58, 1–18, <https://doi.org/10.2138/rmg.2005.58.1>, 2005.](#)
- Rocklin, M.: Dask: Parallel computation with blocked algorithms and task scheduling, *Proceedings of the 14th Python in Science Conference*, 130–136, 2015.
- 640 Rybacki, E., Gottschalk, M., Wirth, R., and Dresen, G.: Influence of water fugacity and activation volume on the flow properties of fine-grained anorthite aggregates, *Journal of Geophysical Research: Solid Earth*, 111, <https://doi.org/10.1029/2005JB003663>, 2006.

- Sandiford, D., Brune, S., Glerum, A., Naliboff, J., and Whittaker, J. M.: Kinematics of Footwall Exhumation at Oceanic Detachment faults: Solid-Block Rotation and Apparent Unbending, *Geochemistry, Geophysics, Geosystems*, 22, e2021GC009681, <https://doi.org/10.1029/2021GC009681>, 2021.
- 645 Shuster, D. L., Flowers, R. M., and Farley, K. A.: The influence of natural radiation damage on helium diffusion kinetics in apatite, *Earth and Planetary Science Letters*, 249, 148–161, <https://doi.org/10.1016/j.epsl.2006.07.028>, 2006.
- Sullivan, C. B. and Kaszynski, A. A.: PyVista: 3D plotting and mesh analysis through a streamlined interface for the Visualization Toolkit (VTK), *Journal of Open Source Software*, 4, 1450, <https://doi.org/10.21105/joss.01450>, 2019.
- 650 Tamer, M. and Ketcham, R.: Is Low-Temperature Fission-Track Annealing in Apatite a Thermally Controlled Process?, *Geochemistry, Geophysics, Geosystems*, 21, e2019GC008877, <https://doi.org/10.1029/2019GC008877>, 2020.
- Ternois, S., Mouthereau, F., and Jourdon, A.: Decoding low-temperature thermochronology signals in mountain belts: modelling the role of rift thermal imprint into continental collision, *Bulletin de la Société Géologique de France*, 192, 38, <https://doi.org/10.1051/bsgf/2021028>, 2021.
- Thieulot, C.: ELEFANT: a user-friendly multipurpose geodynamics code, *Solid Earth Discussions*, 6, 1949–2096, <https://doi.org/10.5194/sed-6-1949-2014>, 2014.
- Vasey, D. and Scully, P., and Stoner, R.: dyvasey/gdtchron: GDTchron 0.1.1-2, <https://doi.org/10.5281/zenodo.17914931>, 2025, [17914931](https://doi.org/10.5281/zenodo.17914931), [202518602490](https://doi.org/10.5281/zenodo.202518602490), 2026.
- Vasey, D. A., Naliboff, J. B., Cowgill, E., Brune, S., Glerum, A., and Zwaan, F.: Impact of rift history on the structural style of intracontinental rift-inversion orogens, *Geology*, 52, 429–434, <https://doi.org/10.1130/G51489.1>, 2024.
- 660 Vincent, S. J., Braham, W., Lavrishchev, V. A., Maynard, J. R., and Harland, M.: The formation and inversion of the western Greater Caucasus Basin and the uplift of the western Greater Caucasus: Implications for the wider Black Sea region, *Tectonics*, 35, 2948–2962, <https://doi.org/10.1002/2016TC004204>, 2016.
- Vincent, S. J., Somin, M. L., Carter, A., Vezzoli, G., Fox, M., and Vautravers, B.: Testing Models of Cenozoic Exhumation in the Western Greater Caucasus, *Tectonics*, 39, e2018TC005451, <https://doi.org/10.1029/2018TC005451>, 2020.
- 665 Virtanen, P., Gommers, R., Oliphant, T. E., Haberland, M., Reddy, T., Cournapeau, D., Burovski, E., Peterson, P., Weckesser, W., Bright, J., van der Walt, S. J., Brett, M., Wilson, J., Millman, K. J., Mayorov, N., Nelson, A. R. J., Jones, E., Kern, R., Larson, E., Carey, C. J., Polat, I., Feng, Y., Moore, E. W., VanderPlas, J., Laxalde, D., Perktold, J., Cimrman, R., Henriksen, I., Quintero, E. A., Harris, C. R., Archibald, A. M., Ribeiro, A. H., Pedregosa, F., and van Mulbregt, P.: SciPy 1.0: fundamental algorithms for scientific computing in Python, *Nat Methods*, 17, 261–272, <https://doi.org/10.1038/s41592-019-0686-2>, 2020.
- 670 Willett, S., Beaumont, C., and Fullsack, P.: Mechanical model for the tectonics of doubly vergent compressional orogens, *Geology*, 21, 371–374, [https://doi.org/10.1130/0091-7613\(1993\)021%253C0374:MMFTTO%253E23E2.3.CO;2](https://doi.org/10.1130/0091-7613(1993)021%253C0374:MMFTTO%253E23E2.3.CO;2), 1993.
- 675 Wolf, S. G., Huisman, R. S., Muñoz, J.-A., Curry, M. E., and van der Beek, P.: Growth of Collisional Orogens From Small and Cold to Large and Hot—Inferences From Geodynamic Models, *Journal of Geophysical Research: Solid Earth*, 126, e2020JB021168, <https://doi.org/10.1029/2020JB021168>, 2021.
- Yamada, R., Murakami, M., and Tagami, T.: Statistical modelling of annealing kinetics of fission tracks in zircon: Reassessment of laboratory experiments, *Chemical Geology*, 236, 75–91, <https://doi.org/10.1016/j.chemgeo.2006.09.002>, 2007.

680 Yuan, X. P., Braun, J., Guerit, L., Rouby, D., and Cordonnier, G.: A New Efficient Method to Solve the Stream Power Law Model Taking Into Account Sediment Deposition, *Journal of Geophysical Research: Earth Surface*, 124, 1346–1365, <https://doi.org/10.1029/2018JF004867>, 2019a.

Yuan, X. P., Braun, J., Guerit, L., Simon, B., Bovy, B., Rouby, D., Robin, C., and Jiao, R.: Linking continental erosion to marine sediment transport and deposition: A new implicit and  $O(N)$  method for inverse analysis, *Earth and Planetary Science Letters*, 524, 115728, <https://doi.org/10.1016/j.epsl.2019.115728>, 2019b.

685 Zwaan, F., Brune, S., Glerum, A. C., Vasey, D. A., Naliboff, J. B., Manatschal, G., and Gaucher, E. C.: Rift-inversion orogens are potential hot spots for natural H<sub>2</sub> generation, *Science Advances*, 11, eadr3418, <https://doi.org/10.1126/sciadv.adr3418>, 2025.